Journal of Power Sources 195 (2010) 7634–7638

Contents lists available at ScienceDirect

Journal of Power Sources

journal homepage: www.elsevier.com/locate/jpowsour

Short communication

Model-based distinction and quantification of capacity loss and rate capability fade in Li-ion batteries

Alexander P. Schmidt[a,*], Matthias Bitzer[b], Árpád W. Imre[a], Lino Guzzella[c]

[a] Robert Bosch GmbH, Corporate Research, Electric Vehicle – System & Components, Robert-Bosch-Strasse 2, D-71701 Schwieberdingen, Germany
[b] Robert Bosch GmbH, Corporate Research, Control Theory, Robert-Bosch-Strasse 2, D-71701 Schwieberdingen, Germany
[c] Institute for Dynamic Systems and Control (IDSC), ETH Zurich, Sonneggstrasse 3, CH-8092 Zurich, Switzerland

ARTICLE INFO

Article history:
Received 16 March 2010
Received in revised form 26 April 2010
Accepted 2 June 2010
Available online 15 June 2010

Keywords:
Electrochemical battery modeling
SOH estimation
Online parameter estimation
Solid–electrolyte interface
Electrolyte dissociation

ABSTRACT

This work is focused on an easy-to-handle approach for estimating the residue power and capacity of a lithium-ion cell during operation. For this purpose, an earlier presented lumped parameter electrochemical battery model is employed. By means of the parameters accounting for the cathode capacity and the electrolyte conductivity, the cell degradation is successfully reproduced. Moreover, the method enables the distinction of capacity fade due to impedance rise and due to active material loss. High discharge rates together with the correlated self-heating of the cell enable a model-based quantification of SEI and electrolyte contributions to the overpotential.

1. Introduction

The accurate and reliable prediction of available power and energy is a challenging task for battery management systems (BMS) in future electrochemical storage devices. This is based on mainly two issues. First, lower and upper cut-off voltages must be maintained for safety reasons [1]. Further on, it is exceedingly desirable to fully exploit the installed capacity and thus, save cell costs.

Recently, an advanced lumped parameter physics-based battery model was proposed by the authors [2]. This model forms a promising basis for sophisticated functionalities such as an exact state of charge (SOC) and state of health (SOH) prediction. Since the most state variables such as SOC are not accessible to measurements [1,3], a state estimator is required for online applications. Moreover, the reliable prediction of available power and capacity is intrinsically tied to an accurate parameter set. Unfortunately, lithium-ion cells are subject to a significant loss of capacity and rate capability fade during cyclic operation [4,5] as well as during longer rest phases of several weeks or months. Consequently, in the case of a model-based BMS, the parameter set has to be checked regularly in order to preserve the fidelity of the employed algorithm. In consideration of the fact that physical models incorporate 30–80 constant parameters [2], this raises the question which are the model parameters that are significantly affected by the cell degradation.

The idea of addressing cell aging to only a few parameters of an electrochemical battery was first proposed in [6] by means of empirical models for the SOC, the solid electrolyte film resistance, and the solid state diffusion coefficient of the anodic active material. Based on these considerations conducted in [6], the paper at hand discusses the monitoring of only two parameters which were found to be especially sensitive for cell aging. In contrast to [6], the identification of the parameters is done by means of a lumped electrochemical battery model [2]. The investigations are extended to high discharge rates, i.e. $I = 8C$. This allows to quantify the contribution of the electrolyte conductivity to the overpotential.

In the following, an easy-to-handle algorithm is developed that allows for the online monitoring of the cell's state of health. This becomes feasible by the lumped parameter structure of the employed battery model. The capacity loss and the rate capability fade is well reproduced by means of the tracing of two key parameters during cyclic operation. This is achieved by employing a state of the art state estimator for nonlinear systems in combination with recurrent identical load cases. The simulated predictions in the SOH have been verified using experimental data of a high-power lithium-ion cell that was cycled in a high temperature regime.

* Corresponding author. Tel.: +49 711 81134050; fax: +49 711 81151824787.
E-mail addresses: alexander.schmidt7@de.bosch.com (A.P. Schmidt), matthias.bitzer2@de.bosch.com (M. Bitzer), arpad.imre@de.bosch.com (Á.W. Imre), lguzzella@ethz.ch (L. Guzzella).
URL: http://www.idsc.ethz.ch (L. Guzzella).

0378-7753/$ – see front matter © 2010 Elsevier B.V. All rights reserved.
doi:10.1016/j.jpowsour.2010.06.011

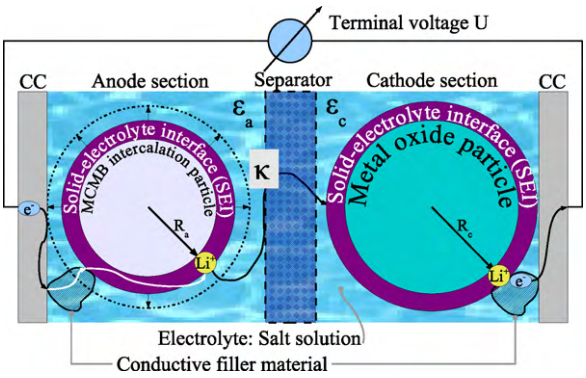

Fig. 1. Visualization of the proposed lithium-ion battery model. The electrochemical cell structure is connected to the external load circuit by the current collectors denoted by CC.

2. Determination of key parameters for cell degradation

2.1. Battery cell model and aging effects

The named extended lumped parameter model [2] consists of one representative intercalation particle for each electrode, see Fig. 1. The SOC is defined as the ratio of the currently stored amount of charge in these particles to the physically accessible maximum value. The Butler–Volmer reaction kinetics equation [7] is used for the charge transfer across the particle/electrolyte interface. Further on, diffusion and migration of lithium-ions are assumed to occur in the electrolyte. Within this work, the ion transport between the active particles is characterized by an effective conductivity. The law of Arrhenius, see [8] for instance, is used to describe the observed temperature dependence of the velocity of the electrolyte and solid-phase ion transport as well as of the reaction kinetics. A temperature balance accounting for ohmic heating as source term and for radiation as well as convection as heat sinks yields the actual temperature of the cell. Finally, the terminal voltage and the averaged cell temperature represent the responses of the system to an excitation with an external load current in charge or discharge direction.

It is known that the metal oxide cathode is much more subject to capacity losses than the mesocarbon microbead (MCMB) anode [9,10]. Therefore, within this work a degradation is considered only for the cathode, whereas the aging of the anode is neglected for simplicity. The actual capacity can be expressed by the model parameter porosity ε_c of the cathode. It can be determined according to [2] as

$$\varepsilon_c = K_1 \frac{1}{dSOC/dt} I, \tag{1}$$

where K_1 is a constant typical for the respective intercalation particle, and I is the externally applied current [2]. The porosity ε_c accounts for the volume fraction of intercalation particles in the cathode. During the operation of the cell, some particles will crack [11–13] or simply be isolated from the conductive matrix [5]. These degraded regions then reduce the effective porosity ε_c and thus, the capacity of the respective electrode. Obviously, in the model presented, see Fig. 1, the porosity ε_c is of abstract nature since only one representative particle is considered. The porosity actually operates as a scaling factor for the ratio of volume filled by intercalation material to the total volume of the electrode.

With increasing (cyclic) age of the cell, an increase in the overpotential is observed [5]. With respect to the proposed model, this issue might be addressed to (i) the continuous growth of an anodic solid–electrolyte interface (SEI) layer [6,14] and/or (ii) to a reduced conductivity κ between the active materials, see Fig. 1. The SEI layer on the cathode is considered to be circumstantial [4,10,15]. When applying material properties and growth dynamics as reported in [16] for instance, the authors found the anodic SEI film resistance to be of subsidiary relevance for the rate capability decrease, too. By contrast, a decrease of the effective electrolyte conductivity κ provides a very well reproduction of the power capability fade. A respective statement considering the degradation of the electrolyte as continuous process in the cell can be found in [14], as wells as concrete side reaction equations. The following result newly allows for the model-based quantification of the electrolyte degradation. The variable κ shows a temperature dependence according to the law of Arrhenius where only the preexponential factor is subject to aging. The respective activation energy $E_{0,L} = 15.4\,\mathrm{kJ\,mol^{-1}}$ has been determined in the course of [2] and suggests that κ accounts for the conductivity of a liquid [17], i.e. the electrolyte, to the most extent. This correlation is visible first, when the applied load current causes a significant self-heating of the cell of more than 10 K. The conductivity κ can be readily computed by utilizing the temperature balance presented in [2], i.e.

$$\frac{dT}{dt} = K_5 \left(f_5(T) + \frac{1}{A_s} U_{OV}(\boldsymbol{x}, I, \kappa) I \right), \tag{2}$$

where the surface overpotential difference U_{OV} [6,2] reads as

$$U_{OV}(\boldsymbol{x}, I, \kappa) = \Delta\Phi_{BV}(\boldsymbol{x}, I) + \Phi_{\mathrm{SEI},a}(T, I) + \Phi_{\mathrm{SEI},c}(T, I) + \underbrace{\kappa^{-1} f_7(T, I) + f_8(\boldsymbol{x}, I)}_{=:\Phi_2}, \tag{3}$$

with $\Delta\Phi_{BV}$ accounting for the potential contribution of the Butler–Volmer reaction kinetics, $\Phi_{\mathrm{SEI},a/c}$ for the SEI film layer potential drops and Φ_2 for the electrolyte potential. Obviously, Eqs. (2) and (3) contain the internal state vector $\boldsymbol{x} = [\overline{q}_a, \overline{q}_c, \mathrm{SOC}_a, \mathrm{SOC}_c, T, c_{el}]^T$ of the battery model [2]. The variables $\overline{q}_a$, $\overline{q}_c$ account for the volume averaged flux of lithium-ions in the active particles, the variables SOC_a, SOC_c for the bulk state of charge of these particles, and T is the cell temperature. The state c_{el} represents the electrolyte lithium-ion concentration.

Summarizing, the parameters cathodic porosity ε_c and effective electrolyte conductivity κ are employed as key parameters in order to estimate the rate capability fade and the capacity loss of the cell as follows. The rate capability fade ΔR is directly expressed by the increase of the electrolyte conductivity, i.e.

$$\Delta R = \kappa^{-1} - \kappa_0^{-1} \tag{4}$$

with κ_0 being the respective conductivity for a fresh battery. The actual capacity $C_{tot,est}$ of the cell is determined according to

$$C_{tot,est} = \underbrace{\frac{\varepsilon_c}{\varepsilon_{c,0}} C_0}_{=:C_{\varepsilon_c}} - \Delta C_\kappa, \tag{5}$$

where C_0 is the capacity of the new cell. The variable C_{ε_c} represents the capacity fade due to loss of active insertion material and cycleable lithium. The capacity fade ΔC_κ caused by a declined conductivity of the electrolyte is determined by

$$\Delta C_\kappa = f_7(T_{\mathrm{avg}}, I)(\kappa^{-1} - \kappa_0^{-1}) I \tau_{8C,i}, \tag{6}$$

where a discharge with a current of $I = 8C$ is assumed. The variable $\tau_{8C,i}$ denotes the discharge time for the respective cycle number i. For convenience, the cell temperature in the term f_7 is set to the average value $T = T_{\mathrm{avg}}$ during the discharge phase.

2.2. Online degradation estimation

The core idea is to perform congeneric and repeated load profiles during different aging stages of the cell. Neglecting noise processes,

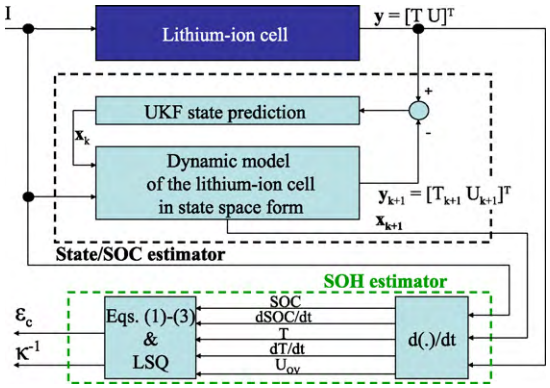

Fig. 2. Schematic drawing of the proposed algorithm to determine the parameters ε_c and κ for the calculation of the power and capacity fade. Since the computations are done in discrete-time domain, the notation $d(\cdot)/dt$ is of symbolic nature.

the shift in respective measured signals for different load cycles numbers can then be addressed to a shift in the two aging-relevant parameters ε_c and κ according to Eqs. (1)–(3). These parameters are estimated by means of a least squares approach [18], and by the measured quantities load current I, terminal voltage U, and cell temperature T. The internal state vector $\boldsymbol{x}$ of the battery model [2] is required within the terms $\Delta\Phi(\boldsymbol{x}, I)$, $f_8(\boldsymbol{x}, I)$ in Eq. (3), and for the determination of $d\mathrm{SOC}/dt$ in Eq. (1). Here, the values of the state vector $\boldsymbol{x}$ are accessed by means of an Unscented Kalman Filter approach (UKF) [19]. The UKF is operated with the nominal parameters $\varepsilon_{c,0}$ and κ_0 that represent a new cell. This approach exploits the fact that state estimators in general compensate model uncertainties to a certain extent such that unmeasured signals converge towards their true physical values.[1] The shifts in parameters relevant for aging are extremely slow when compared to the charge/discharge dynamics of the cell. A measurable variation in ε_c and κ does typically not show up before the completion of a number of $n \geq 5$ load cycles. Practically, the following steps according to Fig. 2 are conducted:

1. Compare estimated states for congeneric load profiles but different aging stages.
2. If there occurs a shift in the values, it must be related to capacity loss and rate capability fade.
3. Compute ε_c and κ using a least squares (LSQ) approach [18] by means of Eqs. (1)–(3) for a respective load cycle, see Fig. 2.
4. Calculation of the residue capacity $C_{tot,est}$ according to Eq. (5).

3. Experimental validation

3.1. Cycling behavior of the cell

In order to accelerate the degradation of the lithium-ion cell during operation, the cycling has been performed in an increased ambient temperature regime. Therefore, the employed climate chamber was set to $T_\infty = 338$ K, i.e. to 65 °C. In Fig. 3, the discharge phase with $I = 8C$ is depicted as a cut-out of the whole load cycle and given examplarily for the 10th and the 385th cycle. The measured data are compared to the simulation model that has been parameterized offline. Thereby, the values for ε_c and κ have been optimized independently every 5 cycles [2]. During this high temperature

[1] During preliminary testing, the applied UKF succeeded to converge without a parameter update until the end of the 385 cycling experiments, where the cell investigated had lost more than 35% of its initial capacity. Usually, a cell is considered to be at its end of life when the residue capacity has declined to 80% of the initially available amount of charge.

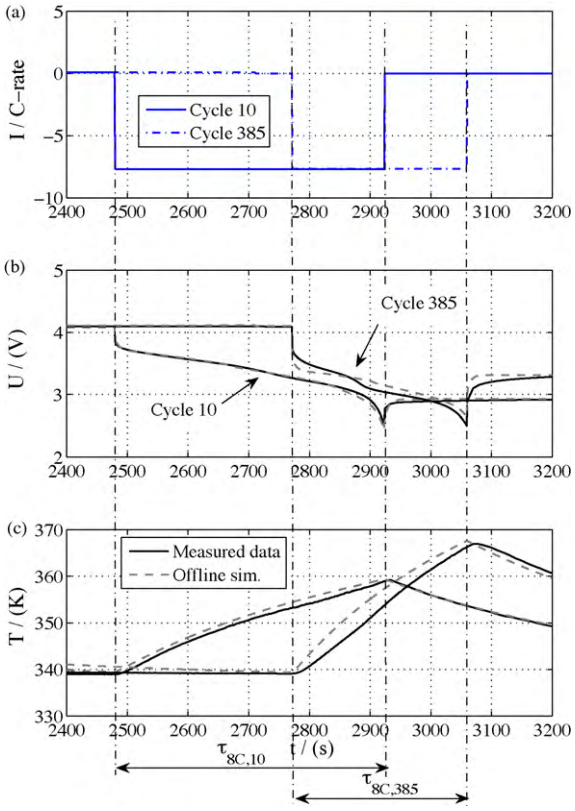

Fig. 3. Comparison of measured data and the model output obtained by means of a offline identification including κ and ε_c.

cycling, the time span τ_{8C} for the 8C discharge clearly decreases and thus, the overall capacity of the cell as well. The variation in the start time of the 8C discharge is due to voltage thresholds of the battery test bench software in combination with the aged cell. The maximum temperature $T_{\max}$ of the cell raises with the cycle numbers, see Fig. 3c. Besides, the quality of a respective offline identification [2] including ε_c and k_c as optimization variables slightly worsens with increasing cycle number as can be seen in Fig. 3b and c. This indicates that ε_c and κ actually cannot cover all but most of the cell aging.

In order to investigate the impact of SEI growth and conductivity loss that might potentially cause an impedance rise, in Fig. 4 the current induced overpotential U_{OV} according to Eq. (3) is employed. It is obvious that during the 8C discharge the overpotential U_{OV} is essentially affected by the electrolyte potential Φ_2 including κ. With parameters as reported in recent publications, see [16] for instance, the SEI layer does not seem to yield a considerably contribution to U_{OV}. Tentatively, an initial anodic SEI film thickness of $d_{\mathrm{SEI},a,10} = 5$ nm with a resistance of $R_{\mathrm{SEI},a} = 0.0017\ \Omega\,\mathrm{m}$ is assumed. Suggesting a film growth up to a layer thickness of $d_{\mathrm{SEI},a,385} = 500$ nm after 385 load cycles, the influence remains neg-

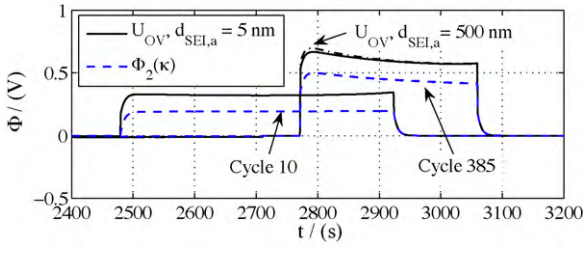

Fig. 4. Contributions of different potentials to the terminal voltage.

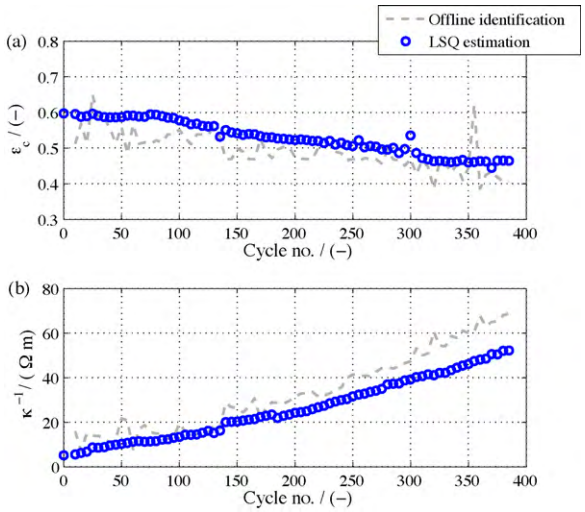

Fig. 5. Development of the estimated values of porosity ε_c and inverse conductivity κ^{-1} during cycling of the cell. The result of the newly proposed algorithm is compared to the data of a respective offline identification scheme.

ligible, see Fig. 4. This model-based examination gives rise to the suggestion to address the capacity fades and rate capability losses to ε_c and κ.

3.2. Quantification and separation of power and capacity fade

Applying the algorithm presented in Section 2.2, the actual values of the cathodic effective porosity ε_c and the effective conductivity κ are computed for every 5th cycle. In Fig. 5 the result is compared with a respective offline parameter identification [2]. Whereas the estimation for ε_c is concordant for both methods, the values for the conductivity κ start to diverge after roughly 150 cycles. Keeping in mind the decreased quality of the offline estimation for an aged cell as depicted in Fig. 3, the values obtained for κ by means of the UKF and LSQ seem to be more reliable. This assumption is confirmed when the cell capacity predicted by the new algorithm as presented in Section 2 is compared to the current integration data of the battery test bench, see Fig. 6. Here, C_{ε_c} is the residue capacity of the cell just considering a degradation of the cathode, i.e. a decrease in ε_c, as shown in Fig. 5a and Eq. (5). The amount of capacity lost by an impedance rise, i.e. ΔC_κ, is computed by the product of the variation in the overpotential U_{OV} due to a rise in κ^{-1}, the actual discharge time span $\tau_{8C,i}$, and the applied load current I, see Eq. (6). The difference $C_{tot,est} := C_{\varepsilon_c} - \Delta C_\kappa$ according to Eq. (5) yields the overall cell capacity $C_{tot,est}$ as estimated according to the algorithm presented in Section 2.2. The result for $C_{tot,est}$ fits the amount of counted ampere hours ($C_{Test\ bench}$) by the battery test bench very well. The error $|C_{Test\ bench} - C_{tot,est}|$ in the predicted cell capacity remains usually below 50 mAh. Related to an initial capacity of $C_0 = 1.26$ Ah, this is equivalent to an upper error bound of less than 5%.

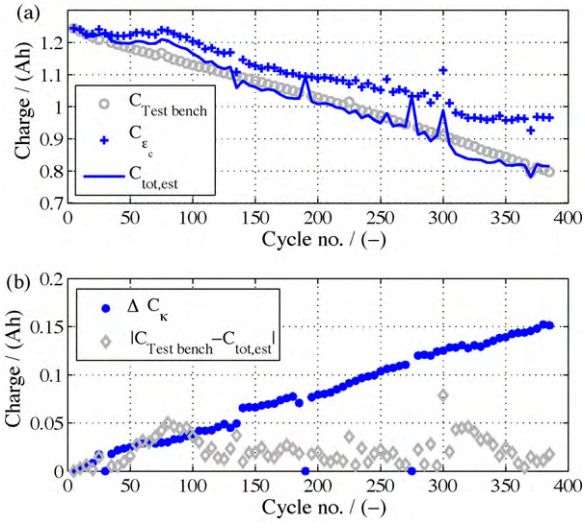

Fig. 6. Contributions to the capacity fade by active material loss (labeled by ε_c) and internal resistance increase (labeled by κ).

4. Conclusion

The application of the algorithm presented yields excellent results for the estimation and quantification of power and capacity fade of a high-power lithium-ion cell. Conducting repeatedly a defined current load profile, the shifts in estimated state variables can be used to determine the SOH of the battery investigated. Moreover, the algorithm presented allows for a clear distinction of the capacity fade due to the degradation of the cathode as well as due to the impedance rise.

The determination of the physical root cause for the impedance rise of the cell is still an open task. If the recently reported material property data and growth behavior of the SEI [16] is confirmed by further researchers, the passivation layer must be excluded from the list of candidates. Although, it seems to be likely that the decomposition of the electrolyte contributes essentially to the rate capability fading, this assumption should be subject to future research.

The excellent robustness of the UKF allows a monitoring of the capacity and rate capability of the cell without a parameter update of the model during battery lifetime. Nevertheless, investigations concerning the independence of parameter and state estimation in the case of regular model updates are a matter of continuative work.

Acknowledgements

We thank Heiko Pape, Joerg Poehler and Bernd Aupperle for their technical support during cell experiments. Further on, the contributions of Robert Cuny and Eric Bauer in the course of their internships at Robert Bosch GmbH are greatly acknowledged. This work was funded by Robert Bosch GmbH, Stuttgart.

References

[1] A. Jossen, W. Weydanz, Moderne Akkumulatoren richtig einsetzen, 1st ed., printyourbook, Germany, 2006.
[2] A.P. Schmidt, M. Bitzer, Á.W. Imre, L. Guzzella, J. Power Sources 195 (2010) 5071–5080.
[3] S. Santhanagopalan, R. White, J. Power Sources 161 (2006) 1346–1355.
[4] M. Broussely, Ph. Biensan, F. Bonhommeb, Ph. Blanchard, S. Herreyre, K. Nechev, R.J. Staniewicz, J. Power Sources 146 (2005) 90–96.
[5] J. Vetter, P. Novák, M.R. Wagner, C. Veit, K.-C. Moeller, J.O. Besenhard, M. Winter, M. Wohlfahrt-Mehrens, C. Vogler, A. Hammouche, J. Power Sources 147 (1-2) (2005) 269–281.
[6] P. Ramadass, B. Haran, R. White, B.N. Popov, J. Power Sources 123 (2003) 230–240.
[7] J. Newman, K. Thomas-Alyea, Electrochemical Systems, 3rd ed., Wiley-Interscience, Hoboken, NJ, 2004.
[8] C.E. Mortimer, U. Mueller, Chemie: das Basiswissen der Chemie, 7th ed., Georg Thieme Verlag, Stuttgart, 2001.
[9] M. Winter, J.O. Besenhard, Electrochim. Acta 45 (1999) 31–50.
[10] J. Christensen, J. Newman, J. Electrochem. Soc. 151 (11) (2004) A1977–A1988.
[11] J. Christensen, J. Newman, J. Solid State Electrochem. 10 (2006) 293–319.
[12] J. Christensen, J. Newman, J. Electrochem. Soc. 153 (6) (2006) A1019–A1030.
[13] X. Zhang, W. Shyy, A.M. Sastry, J. Electrochem. Soc. 154 (10) (2007) A910–A916.
[14] G. Ning, B. Haran, B.N. Popov, J. Power Sources 117 (2003) 160–169.
[15] H.J. Ploehn, P. Ramadass, R.E. White, J. Electrochem. Soc. 151 (3) (2004) A456–A462.

[16] M. Safari, M. Morcrette, A. Teyssot, C. Delacourt, J. Electrochem. Soc. 156 (3) (2009) A145–A153.
[17] V.D. Fedotov, F.M. Samigullin, Z.Sh. Idiyatullin, The activation energy in the thermal motion of liquid molecules, JSTCAM 25 (1) (1984) 221–222.
[18] L. Ljung, System Identification: Theory for the User, Prentice-Hall, Englewood Cliffs, NJ, 1987.
[19] S. Julier, J. Uhlmann, Int. Symp. Aerospace/Defense Sensing, Simul. and Controls, Orlando, FL, 1997.